ISSN 1063-7826, Semiconductors, 2012, Vol. 46, No. 12, pp. 1510–1517. © Pleiades Publishing, Ltd., 2012.
Original Russian Text © S.N. Nikolaev, V.V. Rylkov, B.A. Aronzon, K.I. Maslakov, I.A. Likhachev, E.M. Pashaev, K.Yu. Chernoglazov, A.S. Semisalova, N.S. Perov, V.A. Kul'bachinskii, O.A. Novodvorsky, A.V. Shorokhova, O.D. Khramova, E.V. Khaydukov, V.Ya. Panchenko, 2012, published in Fizika i Tekhnika Poluprovodnikov, 2012, Vol. 46, No. 12, pp. 1546–1553.

XVI SYMPOSIUM
"NANOPHYSICS AND NANOELECTRONICS",
NIZHNI NOVGOROD, MARCH 12–16, 2012

High-Temperature Ferromagnetism of $Si_{1-x}Mn_x$ Films Fabricated by Laser Deposition Using the Droplet Velocity Separation Technique

S. N. Nikolaev[a], V. V. Rylkov[a, e^], B. A. Aronzon[a, f], K. I. Maslakov[b], I. A. Likhachev[a], E. M. Pashaev[a], K. Yu. Chernoglazov[a], A. S. Semisalova[c], N. S. Perov[c], V. A. Kul'bachinskii[a, c], O. A. Novodvorsky[d], A. V. Shorokhova[d], O. D. Khramova[d], E. V. Khaydukov[d], and V. Ya. Panchenko[d]

[a] *National Research Centre "Kurchatov Institute", pl. Kurchatova 1, Moscow, 123182 Russia*
^e-mail: vvrylkov@mail.ru
[b] *Faculty of Chemistry, Lomonosov Moscow State University, Moscow, 119991 Russia*
[c] *Faculty of Physics, Lomonosov Moscow State University, Moscow, 119991 Russia*
[d] *Institute of Laser and Information Technologies, Russian Academy of Sciences, Shatura, Moscow district, 140700 Russia*
[e] *V.A. Kotelnikov Institute of Radio Engineering and Electronics, Fryazino Branch Russian Academy of Sciences, Fryazino, Moscow district, 141190 Russia*
[f] *Institute for Theoretical and Applied Electrodynamics, Russian Academy of Sciences, Moscow, 127412 Russia*

Submitted April 15, 2012; accepted for publication April 25, 2012

Abstract—The transport and magnetic properties of $Si_{1-x}Mn_x$ films of thickness 55–70 nm with various Mn content ($x = 0.44$–0.6) are studied in the temperature range of 5–400 K and in magnetic fields up to 2 T. The films are grown by pulsed laser deposition on Al_2O_3 (0001) substrates at a temperature of 340°C using velocity separation of deposited particles. The films exhibit metal conductivity and the resistivity $\rho = (2–8) \times 10^{-4}\ \Omega$ cm, typical of highly degenerate semiconductors. It is found that the anomalous component of the Hall effect dominates over the normal component at $T = 300$ K for the $Si_{1-x}Mn_x$ alloy with $x \approx 0.5$, and that the Curie temperature significantly exceeds room temperature and is estimated as ~500 K from magnetization measurements (for MnSi silicide the Curie temperature is $T_C = 30$ K). It is shown that the anomalous component of the Hall conductivity at low temperatures is controlled by "side-jump" and (or) "intrinsic" mechanisms independent on the carrier scattering time. The results are explained by features of the formation of defects with localized magnetic moments in the case of $Si_{1-x}Mn_x$ films with $x \approx 0.5$ and by the significant role of matrix spin fluctuations in the exchange between these defects.

DOI: 10.1134/S1063782612120123

1. INTRODUCTION

It is known that the fundamental limitation preventing the efficient spin injection of carriers from ferromagnetic metals to nonmagnetic semiconductors is the strong difference in the conductivities (spin resistivities) of these materials [1–4]. In this context, one of the most important directions in semiconductor spintronics is the development and study of magnetic systems with carrier spin polarization at higher temperatures and relatively high resistivities similar to those of highly degenerate semiconductors ($\rho = 10^{-4}$–$10^{-3}\ \Omega$ cm), i.e., exceeding metal resistivity by several orders of magnitude. Among such systems are magnetic semiconductors (MSs) based on Group-III and -V elements such as GaMnAs [5]. However, despite significant progress in the development of these semiconductors, their Curie temperatures (~170 K) are still appreciably lower than room temperature [5, 6].

Recently, particular attention has also been paid to the development and study of properties of magnetic-semiconductor systems based on elemental semiconductors such as Si, in particular, $Si_{1-x}Mn_x$ alloys, since such materials are attractive for developing spintronic elements easily integrated into the existing microelectronic technology [7]. From the fundamental point of view, $Si_{1-x}Mn_x$ alloys are of interest due to their extraordinary magnetic properties which cannot be described within known models (in particular, the RKKY–Zener models), used in the case of magnetic semiconductors such as GaMnAs, or are explained only by Mn-silicide formation with Curie temperatures $T_C < 50$ K (see [8] and references therein).

Recently, in $Si_{1-x}Mn_x$ films ($x \approx 0.35$, $\rho \approx 2 \times 10^{-4}$ Ω cm) grown by pulsed laser deposition (PLD), we detected ferromagnetism (FM) at room temperature, which is accompanied by the anomalous Hall effect (AHE), indicating the existence of carrier spin polarization [9, 10]. The results obtained were interpreted within a model [8] based on an assumption regarding the formation of a Mn_4Si_7 silicide matrix,[1] containing magnetic defects due to its non-stoichiometry, whose exchange via spin fluctuations (paramagnons) of the matrix leads to a strong increase in T_C of the $Si_{1-x}Mn_x$ films [10]. Further studies showed that the development of well-reproducible magnetic systems based on Mn_4Si_7 is problematic due to the diversity of the stable phases of higher silicides (no less than five) such as $MnSi_y$ with close component content ($y = 1.72$–1.75).

In this work, we study the possibility of growing the $Si_{1-x}Mn_x$ ferromagnetic films by the PLD method with the other value of $x \approx 0.5$, i.e., close to that of MnSi monosilicide whose composition differs appreciably from both higher (Mn_4Si_7, $Mn_{11}Si_{19}$, $Mn_{15}Si_{26}$, and others) and lower manganese silicides (Mn_5Si_3, Mn_5Si_2). Therefore, it is less probable to obtain a structurally inhomogeneous material representing a mixture of individual silicide types. It is also important that MnSi is a weak itinerant ferromagnet in which, at $T > T_C \approx 30$ K, the role of spin fluctuations is great [12], and the appearance of high-temperature FM similar to that revealed in studies [8, 10] can be expected in the presence of magnetic defects localized in the MnSi matrix.

It was found that the anomalous Hall effect in the $Si_{1-x}Mn_x$ alloy at $x \approx 0.5$ at $T = 300$ K is almost five times stronger than in $Si_{1-x}Mn_x$ with $x \approx 0.35$, and the Curie temperature substantially exceeds room temperature ($T_C \geq 400$ K). In this case, the resistivity of the films exhibiting high-temperature FM is $(2$–$8) \times 10^{-4}$ Ω cm, i.e., is typical of highly degenerate semiconductors.

2. SAMPLES AND METHODS FOR THEIR STUDY

The $Si_{1-x}Mn_x$ films of thickness 55–70 nm with various Mn content ($x = 0.44$–0.6) were grown by pulsed laser deposition using velocity separation of deposited particles [13] and with a controlled energy spectrum of laser erosion plume ions [14]. The method [13] makes it possible to completely avoid the arrival of drops at the growing film, whose presence is the major factor in their quality decrease when using PLD. In particular, ZnO:Ga films grown by the PLD method using a separator, exhibited epitaxial quality [15]. It is also important that the surface roughness of Si films grown in a similar way did not exceed 1 nm [14]. The layers were deposited on Al_2O_3 (0001) substrates at a temperature of 340°C with a rate of 1.5 nm/min.

Using precision masks, the $Si_{1-x}Mn_x/Al_2O_3$ structures were fabricated in the form of a double Hall bar (the alignment accuracy of the Hall probes is no worse than 10 μm) to study the conductivity and Hall effect, with a conducting channel width of $W = 1.2$ mm and a spacing between the potential probes of $L = 1.4$ mm.

The masks also allowed the fabrication of rectangular samples 4.4 × 5 mm in size to study the composition and structural properties of the films.

The film composition was studied by X-ray photoelectron spectroscopy (XPS) using a Quantera SXM spectrometer (Physical Electronics Co.). The measurements were performed in a vacuum chamber with a residual pressure of $\sim 10^{-8}$ mbar after cleaning the film surfaces by argon ions with an energy of 2 kV for 30 and 60 s. The thickness of the removed layer in the cleaning time is 5–10 nm.

The structural properties of the samples were studied using θ–2θ scanning using a Rigaku SmartLab X-ray diffractometer with a parabolic X-ray mirror without monochromators and without slits in front of the detector. Therefore, the incident radiation spectrum contained characteristic lines $CuK_{\alpha 1}$, $CuK_{\alpha 2}$, and $CuK_{\beta 1}$. In this case, the direct beam intensity was 1.5×10^9 pulse/s.

The field dependence of the $Si_{1-x}Mn_x$ sample magnetization was measured using a VSM Lake Shore 7407 vibrating sample magnetometer (with a sensitivity of 10^{-5} emu) in fields up to 15 kOe in the temperature range of 100–400 K.

The field during the measurements was parallel to the sample plane. The obtained curves $M(H)$ were processed in two stages. First, the diamagnetic component linear in the field related to the signal from the sample holder and substrate was subtracted from the measured dependence of the magnetic moment. Then, the obtained curves corresponding to the ferromagnetic component of the magnetic moment were divided by the sample volume, after which the found magnetizations were approximated by the Langevin function. Such an approach allows one to distinguish a rather narrow hysteresis loop (~10 Oe) under conditions of a "noisy" weak magnetization signal and to determine with sufficient accuracy the saturation magnetization M_s.

The conductivity and Hall effect of the $Si_{1-x}Mn_x$ samples were measured using an automated setup with an evacuated insert with a superconducting solenoid, immersed in a transport helium Dewar flask, in the temperature range of 5–100 K in a magnetic field up to 2.5 T. The measurements at relatively high temper-

[1] According to available ab initio calculations, Mn_4Si_7 is an indirect-gap semiconductor whose band gap can significantly decrease in the presence of stacking faults and appearing strains [11].

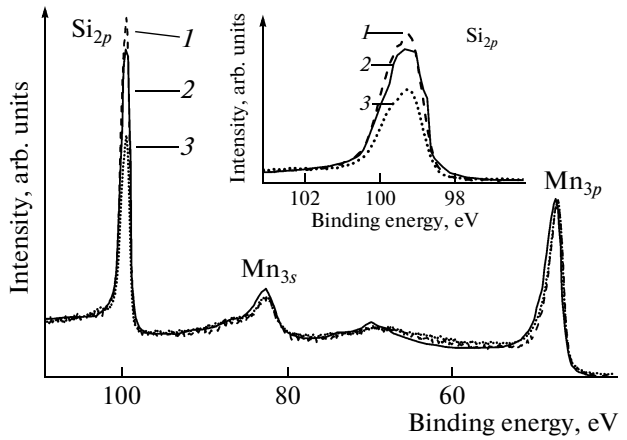

Fig. 1. Comparison of X-ray photoelectron spectra of the Si_{2p} and Mn_{3p} lines for samples 1 $Si_{1-x}Mn_x$ ($x \approx 0.44$) and 3 ($x \approx 0.55$) after cleaning by argon for 60 s (curves *1* and *3*, respectively) with the spectra for the MnSi single crystal (curve *2*), taken from [19]. The inset shows the scaled-up spectra of the Si_{2p} line.

atures (77–300 K) were performed in a nitrogen Dewar flask. In this case, a magnetic field ($B < 1$ T) was induced by an electromagnet.

In the measurements of the Hall effect the voltage between the Hall (V_y) and potential (V_x) probes and the current I_x through the sample were synchronously measured (in the digital form) at various magnetic field polarities during field scanning in the negative and positive directions (as in the magnetization measurements). The longitudinal $R_{xx} = V_x/I_x$ and lateral $R_{xy} = V_y/I_x$ resistances of the sample were determined by the measurement results. The function R_{xy} measured at various polarities of B was expanded in odd and even components,

$$R_H(B) = [R_{xy}^{Down}(B) - R_{xy}^{Up}(-B)]/2, \quad (1)$$

$$R_a(B) = [R_{xy}^{Down}(B) + R_{xy}^{Up}(-B)]/2, \quad (2)$$

where $R_{xy}^{Down}(B)$ and $R_{xy}^{Up}(-B)$ are the lateral resistances corresponding to the "downward" and "upward" directions of field scanning (i.e., in its negative and positive directions); R_H is the Hall resistance, R_a is the asymmetry resistance (even component) caused, in particular, by the non-equipotential arrangement of the Hall probes. Such an approach makes it possible to suppress the parasitic contribution of the magnetoresistive effect to R_{xy}, to distinguish possible hysteresis in the behavior of the Hall resistance [16], and possible even contributions of the incoherent mesoscopic effect or the planar Hall effect [17, 18].

3. RESULTS AND DISCUSSION

3.1. Composition and Structural Properties

The general X-ray photoelectron spectra of the initial sample surface showed that it is contaminated with carbon and oxygen. However, after surface cleaning during 30 s, the carbon and oxygen lines were strongly suppressed. We note special experiments with pure Mn (99.9 at %) plates showed that the appearance of carbon in the spectra is explained by its adsorption on the chemically active surface of films even under conditions of high vacuum ~10^{-8} mbar. Therefore, the carbon contents in the films found by the XPS method can not reflect their actual composition. In this context, the most important parameter was the ratio of silicon and manganese in $Si_{1-x}Mn_x$ films: $y = (1-x)/x$. To calculate y, we used the study of a MnSi single crystal [19], where a clean surface of the single crystal was obtained by its cleavage immediately in the spectrometer's vacuum chamber.

Figure 1 shows the photoelectron spectra of Si_{2p} and Mn_{3p} lines, measured in [19] for the MnSi single crystal and the spectra for two samples J080611 and J211210. The concentration of elements in the samples is proportional to the areas of the corresponding lines. According to the ratio of peak areas, we can see that the silicon content in sample J080611 is higher than in MnSi monosilicide, whereas the situation is reversed for sample J211210. By the ratio of the Si_{2p}- and Mn_{3p}-line areas for the MnSi single crystal, the elemental sensitivity factor was corrected for the Mn_{3p} line in relation to the Si_{2p} line, which was used to calculate the ratio of Si/Mn contents in the $Si_{1-x}Mn_x$ samples. In sample J080611, the ratio $y \approx 1.3$ ($x \approx 0.44$), whereas $y \approx 0.83$ ($x \approx 0.55$) for sample J211210 is significantly less than unity, i.e., film non-stoichiometry toward its Si depletion relative to MnSi silicide is observed in this case (see Fig. 1).

The XPS study of the sample composition allowed the selection of $Si_{1-x}Mn_x$ samples with various Mn contents $x = 0.44$–0.6. Further study was mainly performed for the three most interesting $Si_{1-x}Mn_x$ samples, one of which (J060411) exhibited a component ratio close to MnSi (the estimated value of y is less than unity by several percent); the two others differed from the MnSi composition toward Si enrichment and depletion by $\Delta x/x \approx 10\%$. The parameters of the studied samples are listed in the table. There are also given the Curie temperatures of the samples, found from measurements of the temperature dependence of the magnetization (see subsection 3.2).

That fact that the prepared samples contain MnSi silicide is confirmed by X-ray diffraction studies. The results of X-ray diffraction measurements for the $Si_{1-x}Mn_x/Al_2O_3(0001)$ structure (J060411) are shown in Fig. 2. The diffraction curve contains strong reflection peaks from Al_2O_3 (0006): $2\theta = 41.68°$ for the $CuK_{\alpha 1}$ line, $2\theta = 41.78°$ for the $CuK_{\alpha 2}$ line, and $2\theta = 37.5°$ for the line $CuK_{\beta 1}$. In addition to these peaks,

Parameters of the $Si_{1-x}Mn_x/Al_2O_3(00001)$ structures

Structure	Growth temperature T_g, °C	Film thickness d, nm	Mn content, x	Curie temperatures of the ferromagnetic phases* $T_{C1}(T_{C2})$, K
No. 1 (J080611)	340	55	0.44	FM is absent at $T \geq 100$ K
No. 2 (J060411)	340	70	0.5–0.52	~330
No. 3 (J211210)	340	60	0.55	230 (490)

Note: *Sample 3 (J211210) demonstrates the presence of two ferromagnetic phases.

this curve contains a broad peak from the MnSi (100) film for the CuK_α line at $2\theta = 44.43°$.

The integral characteristic of the film's structural quality is the rocking curve width at half maximum (FWHM). For this film, this parameter is approximately $\Delta\omega = 0.4°$ ($FWHM_\omega$ at $2\theta = 44.43°$), whereas, for a single-crystal film of this thickness the FWHM should be about 250″ [20]. Such a broad peak from the film can indicate significant mosaicity of the structure under study and a large number of crystal defects caused by a low growth temperature and the lattice constant mismatch between Al_2O_3 and MnSi.

3.2. Magnetic Properties

As noted in Section 2, to distinguish the narrow hysteresis loop in the field dependence of the magnetization, the curves $M(H)$ were approximated by the Langevin function. The inset in Fig. 3 shows the field dependence of the magnetization at $T = 300$ K for sample 3 ($x \approx 0.55$), obtained after considering the contribution of the diamagnetic signal from the sample holder and substrate (the field dependence is denoted by symbols *2*). For comparison, the curve calculated using the Langevin function (solid curve) is also shown. We can see that a small hysteresis (the coercivity is ≈100 Oe) appears in the calculated curve, whereas it is difficult to say something about the hysteresis in the experimental function $M(H)$. The temperature dependence of the saturation magnetization for sample 3 ($x \approx 0.55$) is shown in Fig. 3. The dependence $M_s(T)$ for this sample has a distinct bend indicating the existence of two magnetic phases with different Curie temperatures. To estimate T_C of these phases, the temperature dependence of the saturation magnetization was approximated by the often used simplified Brillouin function $M_s(T) = M_s(0)[1 - (T/T_C)^n]$ in which n is usually 1.5–2.5. In the case of two phases,

$$M_s(T) = M_{s1}(0)[1 - (T/T_{C1})^{n_1}] + M_{s2}(0)[1 - (T/T_{C2})^{n_2}], \quad (3)$$

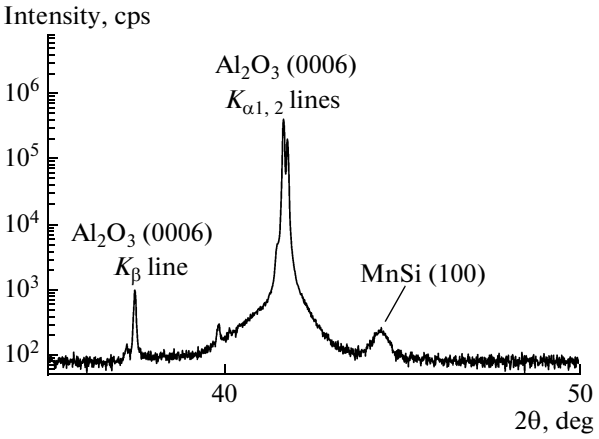

Fig. 2. X-ray diffraction spectrum for structure 2 $Si_{1-x}Mn_x/Al_2O_3$ ($x \approx 0.52$).

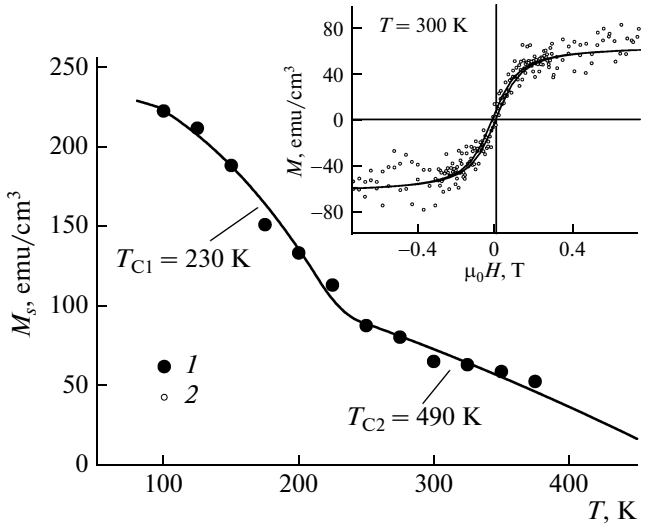

Fig. 3. Temperature dependence of saturation magnetization for structure 3 $Si_{1-x}Mn_x/Al_2O_3$ ($x \approx 0.55$). The symbols *1* denote the experimental data; the solid curve is the approximation using the Brillouin function $M_s(T) = M_{s1}(0)[1 - (T/T_{C1})^{n_1}] + M_{s2}(0)[1 - (T/T_{C2})^{n_2}]$ with $n_1 = 2.5$, $T_{C1} = 230$ K, $n_2 = 1.5$, and $T_{C2} = 490$ K. The inset shows the dependence of the magnetization on the magnetic field for structure 3 $Si_{1-x}Mn_x/Al_2O_3$ ($x \approx 0.55$) at $T = 300$ K. The symbols *2* denote the experimental data; the solid curve was calculated using the Langevin function.

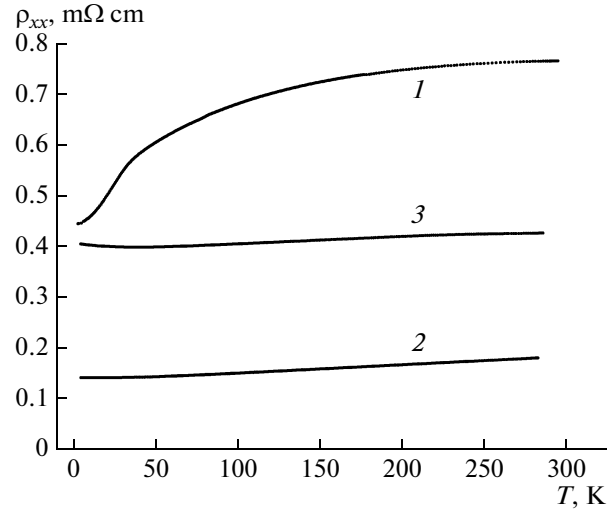

Fig. 4. Temperature dependences of the resistivity for structures 1 $Si_{1-x}Mn_x/Al_2O_3$ ($x \approx 0.44$), 2 ($x \approx 0.52$), and 3 ($x \approx 0.55$) (curves *1*, *2*, and *3*, respectively).

where indices 1 and 2 correspond to low- and high-temperature phases, respectively.

The approximation of the experimental dependence $M_s(T)$ using expression (3) in the case of sample 3 yields $T_{C1} \approx 230$ and $T_{C2} \approx 490$ K. For sample 2 ($x \approx 0.52$) with the least manganese excess and a composition close to MnSi silicide, one phase with $T_{C1} \approx 330$ K appears in the magnetization. In sample 1 ($x \approx 0.44$) with a Mn deficiency (silicon excess), ferromagnetism was not detected in the temperature range $T \geq 100$ K.

It is important that the magnetic moment per manganese atom, estimated by the saturation magnetization for samples 2 and 3 in the limit of low temperatures, is $1.4\mu_B$/Mn and $0.74\mu_B$/Mn, respectively. Meanwhile, for MnSi monosilicide, the moment per Mn atom in the ferromagnetic temperature range appears noticably smaller, ~$0.4\mu_B$/Mn [12], which indicates, according to the model [8], the formation of defects with a localized magnetic moment in the samples with a Mn excess.

It would seem that the anomalous Hall effect should be stronger in sample 3 with the largest manganese excess ($x \approx 0.55$). However, it appeared that the AHE in this sample is controlled by the low-temperature phase and almost disappears at room temperature. Meanwhile, in sample 2 ($x \approx 0.52$) with the least non-stoichiometry, the AHE is observed at $T = 300$ K, and its contribution is dominant in this case, as also at low temperatures (see subsection 3.3).

3.3. Conductivity and Anomalous Hall Effect

In III–Mn–V MSs, as in ferromagnetic metals, the Hall resistance R_H obeys the relation

$$R_H = \frac{R_0}{d}B + \frac{R_s}{d}M, \quad (4)$$

where d is the MS layer thickness, R_0 is the constant of the normal Hall effect caused by the Lorentz force proportional to the magnetic induction B, and R_s is the constant of the anomalous Hall effect controlled by the effect of spin-orbit coupling on spin-polarized carrier transport and proportional to the magnetization M.

The study of the anomalous Hall effect in both single-phase and multiphase or low-dimensional magnetic-semiconductor systems plays a key role in the identification of the ferromagnetic state of these objects [7, 16, 21–23], although the AHE is a rather complex quantum phenomenon, whose nature is still discussed [24]. One of the main causes of such "popularity" is associated with the fact that, for all known mechanisms of the AHE, its observation indicates the existence of spin-polarized carriers in the system, in contrast to observation of the magnetization signal [25]. By the example of III–Mn–V semiconductors, it was shown (see [16] and references therein) that in the presence of the second phase (FM MnAs or MnSb clusters), the magnetization hysteresis indicating the long-range FM order can be observed even above room temperatures. However, in this case, the Hall effect can be normal (linear), caused by the Lorentz force, as in a nonmagnetic semiconductor in the absence of spin-polarized carriers. It is clear that such MSs cannot be used as spin injectors into nonmagnetic semiconductors.

At the same time, as noted in the Introduction, efficient carrier injection into an ordinary semiconductor requires magnetic systems with not only carrier spin polarization at room temperature, but also a relatively high resistivity similar to highly degenerate semiconductors ($\rho = 10^{-4}$–10^{-3} Ω cm). In this context, it is natural to first consider the conductivity of the $Si_{1-x}Mn_x/Al_2O_3$ structures grown by the PLD method.

Figure 4 shows the temperature dependence of the resistivity $\rho_{xx}(T)$ for $Si_{1-x}Mn_x/Al_2O_3$, structure 2 (J060411), with a Mn content $x = 0.5$–0.52 close to that in MnSi silicide. For comparison, the dependences $\rho_{xx}(T)$ for two other samples 1 ($x \approx 0.44$) and 3 ($x \approx 0.55$) are also shown in which this content differs from $x = 0.5$ to the upper and lower sides by 10% (see the table). As expected, the minimum resistivity is observed for sample 2 with the least non-stoichiometry, hence, the least content of structural defects. The structure resistivity decrease with decreasing temperature in the whole range under study, except for structure 3 with $x = 0.55$, in which a small increase in $\rho_{xx}(T)$ is observed below 40 K (see Fig. 4), which indicates weak localization effects. It is important that the room-temperature resistivity of the samples is $\rho = (2$–$8) \times 10^{-4}$ Ω cm which is higher than that of ferromagnetic metals by several orders of magnitude and is typical of highly degenerate semiconductors.

The results of measurements of the dependences of the Hall resistivity for samples 1–3 at various temper-

atures, processed according to the algorithm described in Section 2, are shown in Fig. 5. We can see that the anomalous Hall effect is observed in all the samples at liquid-helium temperatures ($T = 5$–6 K). The maximum value is reached in sample 3 ($x \approx 0.55$, curve *3*); as in sample 2 ($x \approx 0.52$, curve *2*), the AHE is hysteretic. In sample 1 ($x \approx 0.44$, curve *1*), the AHE has the lowest value and is almost completely suppressed even at $T = 64$ K (curve *1'*) with increasing temperature.

It is interesting to note (Fig. 5) that the AHE in sample 3 significantly (twofold) decreases at 197 K (curve *3'*); whereas, in sample 2 whose composition is closest to MnSi, the AHE component remains almost unchanged in this temperature range; compare curves *2* ($T = 6$ K) and *2'* ($T = 197$ K). Moreover, the AHE resistivity ρ_H^a appears approximately five times larger than in previously studied $Si_{1-x}Mn_x$ films with $x \approx 0.35$ [9, 10]. Finally, let us pay attention to the fact that the AHE sign is positive in all samples; whereas AHE < 0 in crystalline MnSi [26], which indicates that there are significant differences between the obtained films and crystalline MnSi silicide.

We recall that two ferromagnetic phases with appreciably differing Curie temperatures were detected in sample 3, whereas only one phase (see the table) appears in the magnetization in sample 2. A noticable change in the AHE for sample 3 in the temperature range of 6–200 K suggests that the high-temperature magnetic phase with $T_{C2} \approx 490$ K is only magnetically active in this case, rather than electrically active (e.g., due to its "discontinuity"). In other words, the AHE for sample 3 is controlled by the low-temperature phase with $T_{C1} \approx 230$ K, and it is natural to associate its severalfold decrease at $T \approx 200$ K with its transition to the paramagnetic state. At the same time, only one phase with $T_C = 330$ K is observed in sample 2 (we recall that $T_C = 30$ K for MnSi [12]). Therefore, the absence of a noticable change in the AHE is quite explainable in the temperature range of 6–200 K.

This conclusion is confirmed by the results of the room-temperature study of the Hall effect using an electromagnet (see the inset in Fig. 5). It follows from the results shown in the inset that the AHE in this case is observed only for sample 2. In other samples, the AHE is absent, the Hall effect is ordinary (linear), caused by the Lorentz force. It is also noteworthy that the resistivity of the anomalous Hall effect in sample 2 at $T = 300$ K is more than five times higher than that of the $Si_{1-x}Mn_x$ alloy at $x \approx 0.35$ (see Fig. 3 in [10]).

To be convinced that the AHE in the case at hand is associated with carrier spin, rather than with ferromagnetic nanoclusters in the samples, whose scattering fields can also lead to anomalies in the Hall effect [25], the mechanism of the latter was additionally studied.

As noted above, the AHE is a complex phenomenon, and at present not all of its mechanisms are quite

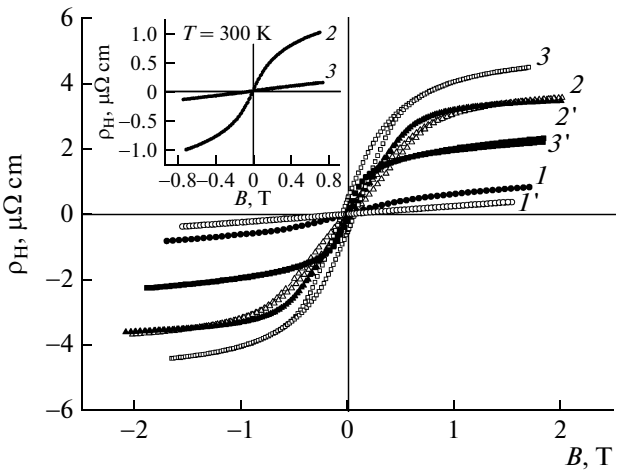

Fig. 5. Dependences of the Hall resistivity ρ_H on the magnetic field for $Si_{1-x}Mn_x/Al_2O_3$ structures: 1 ($x \approx 0.44$) at $T = 5$ K (curve *1*) and $T = 64$ K (curve *1'*); 2 ($x \approx 0.52$) at $T = 6$ K (curve *2*) and $T = 197$ K (curve *2'*); 3 ($x \approx 0.55$) at $T = 6$ K (curve *3*) and $T = 197$ K (curve *3'*). The inset shows the room-temperature dependences of the Hall resistivity ρ_H on the magnetic field for $Si_{1-x}Mn_x/Al_2O_3$ structures: 2 ($x \approx 0.52$) and 3 ($x \approx 0.55$) (curves *2* and *3*, respectively).

understood [24]. This is especially true for materials with low conductivity $\sigma_{xx} < 10^4$ $(\Omega\ \text{cm})^{-1}$, in which unusual scaling was detected for the anomalous component of the Hall conductivity $\sigma_H^a \approx (\rho_H^a/\rho_{xx}^2) \propto \sigma_{xx}^\gamma \propto \tau^\gamma$ with exponent $\gamma = 1.5$–1.6 [24, 27, 28] (ρ_H^a is the anomalous component of the Hall resistivity and τ is the scattering time per pulse). We recall that $\gamma = 1$ (the contribution is proportional to τ) for the known "skew-scattering" mechanism and $\gamma = 0$ (the contribution is independent of τ) in the case of the "side-jump" and "intrinsic" mechanisms [24]. Presumably, such scaling ($\gamma = 1.5$–1.6) is associated with carrier localization effects when approaching the Mott–Anderson metal–insulator transition [24, 28].

The anomalous Hall effect mechanism was studied by the example of sample 3 ($x \approx 0.55$) in which the AHE most strongly varies in the temperature range of 5–200 K (see Fig. 5). The temperature dependence of the resistance of the anomalous Hall component $R_H^a(T, B)$ was measured in strong fields (more than 1 T) corresponding to magnetization saturation. In this case, it is easy to separate the normal and anomalous components from the total resistance $R_H(T, B)$, performing measurements for two magnetic fields B_1, $B_2 > 1$ T (see expression (4)),

$$R_H(T, B) = R_H^n(T, B) + R_H^a(T, B) = \frac{R_0}{d}B + \frac{R_s}{d}M_s(B), \quad (5)$$

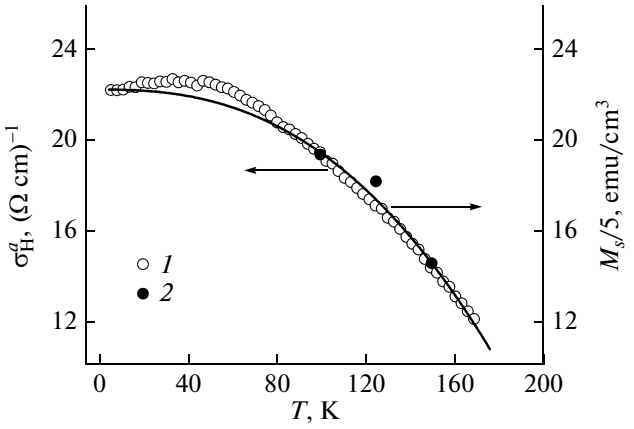

Fig. 6. Temperature dependences of the anomalous component of the Hall conductivity $\sigma_H^a(T)$ for structure 3 $Si_{1-x}Mn_x/Al_2O_3$ ($x \approx 0.55$) (symbols *1*, the left vertical axis). The right vertical axis corresponds to the calculated temperature dependence of the magnetization for the low-temperature phase, found by the data in Fig. 3 using the simplified Brillouin function (the magnetization is fivefold demagnified). The symbols *2* denote the experimental data on the magnetization.

$$dR_H(T) = R_H(T, B_2) - R_H(T, B_1) \approx \frac{R_0}{d}(B_2 - B_1). \quad (6)$$

In relation (6), it is taken into account that $R_H^a(T, B)$ under saturation conditions is independent of the magnetic field.

As in the case of field scanning, even components caused, in particular, by the non-equipotential arrangement of Hall probes and the incoherent mesoscopic effects caused by a change in the carrier flow ways as the temperature changes, can greatly contribute to the measured lateral resistance $R_{xy}(T, B) = V_y/I_x$. Therefore, to separate $R_H(T, B)$ and $R_a(T, B)$ according to (1) and (2), $R_{xy}(T, B)$ were measured at various magnetic field polarities.

Figure 6 shows the temperature dependence of the anomalous component of the Hall conductivity $\sigma_H^a \approx (\rho_H^a/\rho_{xx}^2)$ obtained by measuring the anomalous contribution in the Hall resistance R_H^a. We can see that σ_H^a increases with decreasing temperature and plateaus at $T < 50$ K. Meanwhile, the carrier mobility (hence, the scattering time τ) found by measuring the normal component of the Hall effect increases in this temperature region. Therefore, it is reasonable to assume that σ_H^a is controlled by the intrinsic AHE mechanism (or "side-jump"), is independent of τ, and is defined by the temperature dependence of saturation magnetization [24, 28], $\sigma_H^a(T) \propto M_s(T)$. This is confirmed by comparing the curve $\sigma_H^a(T)$ in this sample with its temperature dependence of the magnetization for the low-temperature phase $M_{s1}(T)$, obtained by the data of Fig. 3 using the simplified Brillouin function (3): $M_{s1}(T) = M_{s1}(0)[1 - (T/T_{C1})^{2.5}]$, where $M_s(0) = 109$ G and $T_{C1} = 230$ K (see Fig. 6). The data of Fig. 6 demonstrate good correlation between the behavior of σ_H^a and $M_{s1}(T)$.

4. CONCLUSIONS

The magnetic and transport properties of Mn_xSi_{1-x} ($x = 0.44$–0.55) films grown on Al_2O_3 (0001) substrates at a temperature of 340°C by pulsed laser deposition using velocity separation of deposited particles were studied. The study was performed in the temperature range of 5–400 K in fields up to 2 T.

It was found that the anomalous Hall effect at $T =$ 300 K for the $Si_{1-x}Mn_x$ alloy with $x \approx 0.5$ is more than five times stronger than for the $Si_{1-x}Mn_x$ alloy with $x \approx 0.35$ [9, 10], and the Curie temperature T_C significantly exceeds room temperature; according to estimations from magnetic measurements, it reaches ~500 K (for MnSi, the Curie temperature is $T_C = 30$ K). It was shown that a change in the Mn content by 10% ($\Delta x \approx \pm 0.05$) results in noticeable ferromagnetism suppression which is substantially stronger for manganese-depleted films. It was shown that the behavior of the anomalous component of the Hall conductivity σ_H^a for samples with $x \approx 0.5$ in a wide temperature range (5–170 K) is unrelated to the "skew-scattering" AHE mechanism, but is more likely controlled by the "side-jump" and (or) "intrinsic" mechanisms independent of the carrier scattering time.

The results are explained by the features of the formation of defects with a localized magnetic moment in the case of $Si_{1-x}Mn_x$ films with $x \approx 0.5$ and the significant role of matrix spin fluctuations (paramagnons) [8] in the exchange between these defects, which lead to a significant increase in the Curie temperature of the $Si_{1-x}Mn_x$ films.

It is also important that the grown films feature metal conductivity and resistivity $\rho = (2$–$8) \times 10^{-4}\ \Omega$ cm typical of highly degenerate semiconductors. The high-temperature ferromagnetism of films, exhibited in the anomalous Hall effect, and their relatively high resistances in comparison with ferromagnetic metals make them attractive for developing injectors of spin-polarized carriers into nonmagnetic semiconductors.

ACKNOWLEDGMENTS

The authors are grateful to V. V. Tugushev for helpful discussions of the ferromagnetism of $Si_{1-x}Mn_x$ alloys.

This study was supported by the Russian Foundation for Basic Research (projects nos. 10-07-00492, 11-07-12063, 11-02-12200, 11-07-12050, 11-02-92478) and the Ministry of Education and Science of the Russian Federation (state contract no. 16.513.11.3088).

REFERENCES

1. G. Schmidt and L. W. Molenkamp, Semicond. Sci. Technol. **17**, 310 (2002).
2. E. I. Rashba, Phys. Rev. B **62**, R16267 (2000).
3. G. Schmidt, D. Ferrand, L. W. Molenkamp, A. T. Filip, and B. J. van Wees, Phys. Rev. B **62**, R4790 (2000).
4. Yu. V. Gulyaev, P. E. Zil'berman, A. I. Panas, and E. M. Epshtein, Phys. Usp. **52**, 335 (2009).
5. T. Jungwirth, J. Sinova, J. Mašek, J. Kucera, and A. H. Mac Donald, Rev. Mod. Phys. **78**, 809 (2006).
6. T. Jungwirth, K. Y. Wang, J. Masek, K. W. Edmonds, J. Konig, J. Sinova, M. Polini, N. A. Goncharuk, A. H. Mac Donald, M. Sawicki, A. W. Rushforth, R. P. Campion, L. X. Zhao, C. T. Foxon, and B. L. Gallagher, Phys. Rev. B **72**, 165204 (2005).
7. S. Zhou and H. Schmidt, Materials **3**, 5054 (2010).
8. V. N. Men'shov, V. V. Tugushev, S. Caprara, and E. V. Chulkov, Phys. Rev. B **83**, 035201 (2011); V. N. Men'shov, and V. V. Tugushev, J. Exp. Theor. Phys. **113**, 121 (2011).
9. S. N. Nikolaev, B. A. Aronzon, V. V. Rylkov, V. V. Tugushev, E. S. Demidov, S. A. Levchuk, V. P. Lesnikov, and V. V. Podolskii, JETP Lett. **89**, 603 (2009).
10. B. A. Aronzon, V. V. Rylkov, S. N. Nikolaev, V. V. Tugushev, S. Caprara, V. V. Podolskii, V. P. Lesnikov, A. Lashkul, R. Laiho, R. R. Gareev, N. S. Perov, and A. S. Semisalova, Phys. Rev. B **84**, 075209 (2011).
11. D. B. Migas, V. L. Shaposhnikov, A. B. Filinov, V. E. Borisenko, and N. N. Dorozhkin, Phys. Rev. B **77**, 075205 (2008).
12. S. M. Stishov and A. E. Petrova, Phys. Usp. **55**, 1117 (2011).
13. O. A. Novodvorskii, A. A. Lotin, and E. V. Khaidukov, Patent RF No. 89906, Byull. No. 35 (2009).
14. E. V. Khaidukov, O. A. Novodvorskii, V. V. Rocheva, A. A. Lotin, D. A. Zuev, and O. D. Khramova, Tech. Phys. Lett. **37**, 69 (2011).
15. O. A. Novodvorskii, L. S. Gorbatenko, V. Ya. Panchenko, O. D. Khramova, E. A. Cherebylo, K. Ventsel', J. V. Barta, V. T. Bublik, and K. D. Shcherbachev, Semiconductors **43**, 419 (2009).
16. V. V. Rylkov, B. A. Aronzon, Yu. A. Danilov, Yu. N. Drozdov, V. P. Lesnikov, K. I. Maslakov, and V. V. Podolskii, J. Exp. Theor. Phys. **100**, 742 (2005).
17. V. V. Rylkov, B. A. Aronzon, A. B. Davydov, D. Yu. Kovalev, and E. Z. Meilikhov, J. Exp. Theor. Phys. **94**, 779 (2002).
18. B. A. Aronzon, A. B. Granovskii, A. B. Davydov, M. E. Dokukin, Yu. E. Kalinin, S. N. Nikolaev, V. V. Rylkov, A. V. Sitnikov, and V. V. Tugushev, J. Exp. Theor. Phys. **103**, 110 (2006).
19. N. Ohtsu, M. Oku, A. Nomura, T. Sugawara, T. Shishido, and K. Wagatsuma, Appl. Surf. Sci. **254**, 3288 (2008).
20. S. Okada, T. Shishido, M. Ogawa, F. Matsukawa, Y. Ishizawa, K. Nakajima, T. Fukuda, and T. Lundstrom, J. Cryst. Growth **229**, 532 (2001).
21. H. Ohno and F. Matsukura, Solid State Commun. **117**, 179 (2001); E. Abe, F. Matsukura, H. Yasuda, Y. Ohno, and H. Ohno, Physica E **7**, 981 (2000).
22. A. M. Nazmul, T. Amemiya, Y. Shuto, S. Sugahara, and M. Tanaka, Phys. Rev. Lett. **95**, 017201 (2005); A. M. Nazmul, S. Sugahara, and M. Tanaka, Phys. Rev. B **67**, 241308 (2003).
23. B. A. Aronzon, V. A. Kul'bachinskii, P. V. Gurin, A. B. Davydov, V. V. Rylkov, A. B. Granovskii, O. V. Vikhrova, Yu. A. Danilov, B. N. Zvonkov, Y. Horikoshi, and K. Onomitsu, JETP Lett. **85**, 27 (2007).
24. N. Nagaosa, J. Sinova, S. Onoda, A. H. Mac Donald, and N. P. Ong, Rev. Mod. Phys. **82**, 1539 (2010).
25. T. Dietl, in *Modern Aspects of Spin Physics*, Lecture Notesin Physics, Vol. 712, Ed. by W. Potz, J. Fabian, and U. Hohenester (Springer-Verlag, Berlin, Heidelberg, 2007), p. 1.
26. M. Lee, Y. Onose, Y. Tokura, and N. P. Ong, Phys. Rev. B **75**, 172403 (2007).
27. T. Fukumura, H. Toyosaki, K. Ueno, M. Nakano, T. Yamasaki, and M. Kawasaki, Jpn. J. Appl. Phys. **46**, L642 (2007).
28. X. Liu, S. Shen, Z. Ge, W. L. Lim, M. Dobrowolska, J. K. Furdyna, and S. Lee, Phys. Rev. B **83**, 144421 (2011).

Translated by A. Kazantsev